World Journal of Engineering Research
Print ISSN: 2959-9865
Online ISSN: 2959-9873
DOI: https://doi.org/10.61784/wjer3074

PRECISE MEASUREMENT OF SILICON CARBIDE EPITAXIAL LAYER THICKNESS BASED ON INFRARED INTERFERENCE PRINCIPLE AND LEAST SQUARES OPTIMIZATION ALGORITHM

Yi Wang
School of Mathematics and Statistics, Hubei University of Education, Wuhan 430205, Hubei, China.

Abstract: This paper focuses on the precise measurement of epitaxial layer thickness in silicon carbide wafers. An ideal mathematical model based on infrared interference and its solution algorithm were constructed and solved. To construct the ideal mathematical model for epitaxial layer thickness measurement, the study first analyzes the physical principles of reflection and refraction of infrared light at the epitaxial layer-substrate interface. Utilizing Snell's law and trigonometric functions, it derives formulas for calculating optical path difference and phase difference. By establishing the conditions for wave interference maxima and minima, the theoretical formula for calculating epitaxial layer thickness was ultimately derived, successfully establishing a mathematical framework under the idealized assumption of only two reflections. Building upon this ideal model, for the thickness measurement algorithm design task, the study first performed standardized preprocessing on the provided spectral data, including S-G smoothing filtering, effectively reducing noise interference. Subsequently, a peak localization and selection algorithm was applied to precisely identify and jointly utilize the extreme points of all 60 interference fringes. To resolve the integer ambiguity issue for interference order m, a traversal optimization algorithm was designed. By searching for the m value that minimizes the variance of the thickness calculation sequence, the optimal interference order was coherently determined. Finally, the least-squares fitting optimization technique yielded an average epitaxial layer thickness of approximately 11.61 μm. A four-dimensional reliability assessment—encompassing parameter sensitivity, data integrity, theoretical consistency, and computational stability—validated the algorithm's exceptional robustness and reliability within the idealized model framework.
Keywords: Silicon carbide epitaxial layer; Infrared interferometry; Least-squares method

1 INTRODUCTION

Silicon carbide (SiC), an emerging compound semiconductor material, finds extensive application in high-performance electronic device manufacturing due to its outstanding high-temperature resistance and tunable optical properties. To achieve specific device performance, a high-quality single-crystal thin film—the SiC epitaxial layer—is typically grown on the SiC substrate surface. Therefore, precise and reliable measurement of the epitaxial layer thickness parameters is crucial for enhancing device performance. The core objective of this study is to establish an ideal mathematical model for measuring epitaxial layer thickness based on infrared interferometry, and to design and implement a thickness calculation algorithm using spectral data along with its reliability assessment. Conventional spectral measurement methods often encounter challenges when processing real data, including high spectral noise, difficulty in determining the interference order m, and insufficient measurement accuracy[1]. The innovation of this section lies in the mathematical model construction, where thickness calculation formulas based on Snell's law and optical path difference were explicitly derived, establishing a solid theoretical foundation for subsequent computations. In algorithm design, S-G filtering was first employed for normalized preprocessing of data, enhancing the signal-to-noise ratio; Second, by jointly utilizing both the maximum and minimum points of interference fringes, the effective data sample size is increased to more than double that of traditional methods. The most critical innovation lies in designing a traversal optimization algorithm. By minimizing the variance of the thickness calculation sequence, it coherently resolves the integer ambiguity problem of the interference order m, significantly enhancing the stability and consistency of the results. The research approach in this section comprises: First, deriving optical path difference and phase difference formulas using geometric optics principles to establish an ideal mathematical model for epitaxial layer thickness calculation; Second, applying S-G filtering and extreme point identification to spectral data provided in the appendix; Finally, a traversal optimization algorithm is designed to determine the interference order m, followed by least-squares optimization for thickness fitting. Comprehensive reliability assessment is conducted across four dimensions: parameter sensitivity, data accuracy, and others[2-3].

2 CONSTRUCTION OF A MATHEMATICAL MODEL FOR EPITAXIAL LAYER THICKNESS MEASUREMENT

2.1 Problem Analysis

We first used GeoGebra to draw a schematic diagram of the epitaxial layer thickness detection principle. Then, we explored the geometric relationships in the diagram based on Snell's Law and trigonometric knowledge to derive the calculation formulas for optical path difference and phase difference. Finally, we established interference conditions to deduce the calculation formula for epitaxial layer thickness[4].
The specific flow chart is as Figure 1:

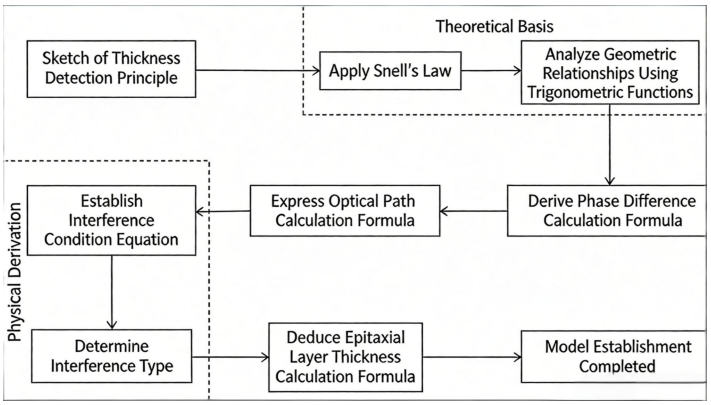

Figure 1 Flow Chart of Problem Analysis

2.2 Model Preparation

After infrared light is incident on the epitaxial layer, part of it is reflected from the surface of the epitaxial layer, and the other part is reflected back from the surface of the substrate. These two beams of light will produce interference fringes under certain conditions. Therefore, the thickness of the epitaxial layer can be determined based on parameters such as the wavelength of the infrared spectrum, the refractive index of the epitaxial layer, and the incident angle of the infrared light.

2.3 Model Establishment

The schematic diagram of the epitaxial layer thickness detection principle is as Figure 2:

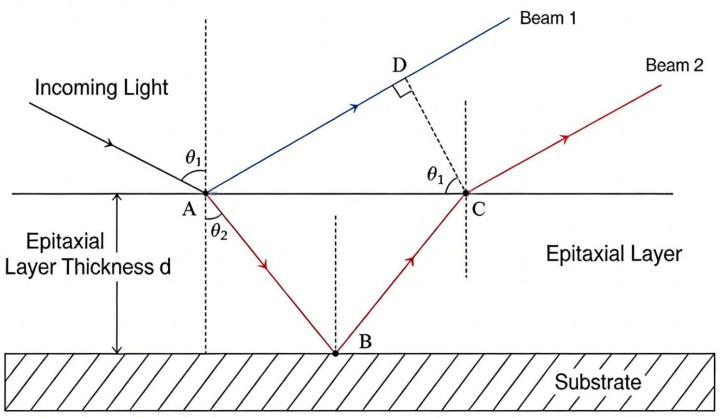

Figure 2 Schematic Diagram of the Epitaxial Layer Thickness Detection Principle

2.3.1 Analysis of Geometric Relationships in Optics

According to Snell's Law, we have:

$$n_1 \sin\theta_1 = n_2 \sin\theta_2 \tag{1}$$

where n_1 is the refractive index of air ($n_1=1$), θ_1 is the incident angle of the incident light, n_2 is the refractive index of the epitaxial layer, and θ_2 is the refraction angle of the incident light[5-6].
Further simplification gives:

$$\sin\theta_1 = n_2 \sin\theta_2 \tag{2}$$

where d is the thickness of the epitaxial layer.

$$L_{AB} = L_{BC} = \frac{d}{\cos\theta_2} \tag{3}$$

$$L_{AC} = 2d\tan\theta_2 \tag{4}$$

$$L_{AD} = L_{AC}\sin\theta_1 = 2d\tan\theta_2 \sin\theta_1 \tag{5}$$

Based on trigonometric knowledge, we obtain:

2.3.2 Calculation Formula for Optical Path Difference

According to the definition of optical path difference and combining the above formulas (2) - (5), the optical path difference of the two reflected beams is:

$$\Delta L=n_2(L_{AB}+L_{BC})-n_1 L_{AD}=2d\sqrt{n_2^2-\sin^2[illegible]\theta_1} \tag{6}$$

2.3.3 Calculation Formula for Phase Difference

The phase difference of the two reflected beams consists of the following two parts:

(1) Reflection phase mutation

The phase change at the interface reflection needs to be considered only when the light wave is incident from an optically denser medium to an optically rarer medium, and a π phase jump occurs at this time. Since beam 1 undergoes a π phase jump at the air-epitaxial layer interface, and beam 2 also undergoes a π phase jump at the epitaxial layer-substrate interface, the relative phase jump is 0. Therefore, the phase difference caused by the reflection phase mutation is:

$$\delta_0=0 \tag{7}$$

(2) Change in optical path difference

According to the interference principle, the change in optical path difference will lead to a change in the phase of the interfering light, and the phase difference is proportional to the optical path difference, satisfying:

$$\delta_1=\frac{2\pi}{\lambda}\Delta L=\frac{4\pi d\sqrt{n_2^2-\sin^2[illegible]\theta_1}}{\lambda} \tag{8}$$

where λ is the wavelength of the light wave in vacuum.

Therefore, the total phase difference is:

$$\delta=\delta_0+\delta_1=\frac{4\pi d\sqrt{n_2^2-\sin^2[illegible]\theta_1}}{\lambda} \tag{9}$$

2.3.4 Establishment of Interference Conditions

(1) Maximum condition for wave interference:

$$\delta=2m\pi\ (m=0,1,2,...) \tag{10}$$

(2) Minimum condition for wave interference:

$$\delta=(2m+1)\pi\ (m=0,1,2,...) \tag{11}$$

2.3.5 Derivation of the Calculation Formula for Epitaxial Layer Thickness

For the special case where the light wave is incident vertically, the incident angle and refraction angle are both 0°. Combining with formula (9), the maximum interference condition can be expressed as:

$$\frac{4\pi dn_2}{\lambda}=2m\pi \tag{12}$$

Simplification gives:

$$d=\frac{m\lambda}{2n_2} \tag{13}$$

For the general case of oblique incidence:

$$d=\frac{m\lambda}{2\sqrt{n_2^2-\sin^2[illegible]\theta_1}} \tag{14}$$

In summary, the calculation formula for the epitaxial layer thickness can be obtained as:

$$d=\frac{m\lambda}{2\sqrt{n_2^2-\sin^2[illegible]\theta_1}} \tag{15}$$

3 ALGORITHM DESIGN FOR EPITAXIAL LAYER THICKNESS MEASUREMENT

3.1 Problem Analysis

We first take the model of problem as the foundation, use the spectral data as known conditions, then establish a set of algorithms based on the calculation formulas of Snell's reflection coefficient and reflectivity combined with the relationship between wavenumber and wavelength, further adopt the least square method [7-8] for data fitting and algorithm optimization, and finally give error analysis to ensure the reliability of the algorithm.

The specific flow chart is as Figure 3:

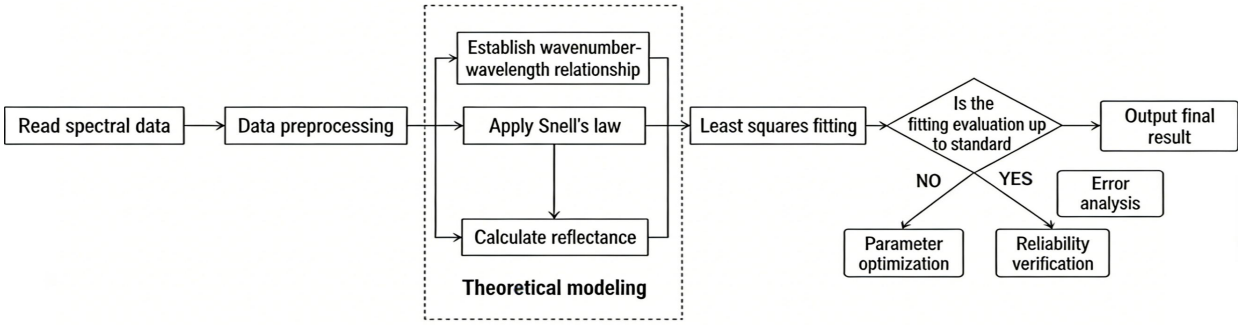

Figure 3 Flow Chart of 3 Algorithm Design for Epitaxial Layer Thickness Measurement

3.2 Basic Theory of the Algorithm

3.2.1 Relationship between wavenumber and wavelength

where $\bar{\nu}$ is the wavenumber and λ is the wavelength.

$$\bar{\nu}=\frac{1}{\lambda} \tag{16}$$

3.2.2 Calculation formulas for snell's reflection coefficients

(1) Snell's reflection coefficient at the air-epitaxial layer interface:

$$r_1=\frac{n_1-n_2}{n_1+n_2} \tag{17}$$

(2) Snell's reflection coefficient at the epitaxial layer-substrate interface:

$$r_2=\frac{n_2-n_3}{n_2+n_3} \tag{18}$$

where n_3 is the refractive index of the substrate.

3.2.3 Calculation formula for reflectivity

Based on the interference of the two reflected beams, the reflectivity formula is:

$$R=\frac{r_1^2+r_2^2+2r_1r_2\cos\delta}{1+r_1^2r_2^2+2r_1r_2\cos\delta} \tag{19}$$

where r_1 is the reflection coefficient at the air-epitaxial layer interface, and r_2 is the reflection coefficient at the epitaxial layer-substrate interface.

3.3 Implementation Steps of the Algorithm

Step 1: Calculate the thickness of the epitaxial layer using the spectral data .
Step 2: Adopt the least square method for data fitting and algorithm optimization to improve the calculation accuracy of the epitaxial layer thickness.
Step 3: Calculate the experimental error and give the necessary analysis to ensure the stability and robustness of the algorithm.

3.4 Solution Results and Analysis of the Algorithm

Based on the aforementioned algorithm flow, we calculated and solved the spectral data. The core of the entire analysis process is to first determine the most reliable interference order sequence through optimization, and then calculate the thickness of the epitaxial layer[9-10].

3.4.1 Data preprocessing and feature extraction

The first step of the algorithm is to preprocess the original data. As can be seen from Figure 4, the original spectral signal has obvious noise. After Savitzky-Golay (S-G) smoothing filtering, the contour of the interference fringes becomes clear and smooth, providing a high-quality data foundation for subsequent extreme point identification.

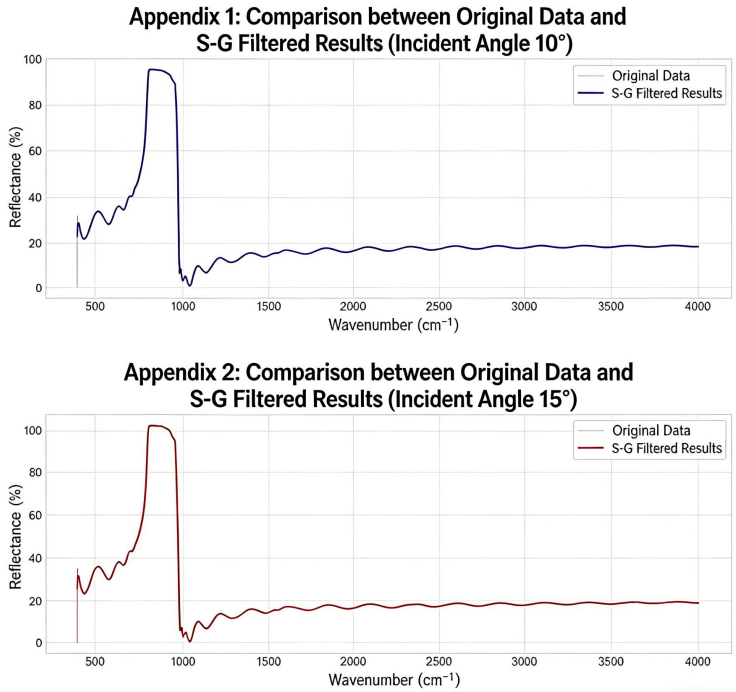

Figure 4 Comparison between Original Reflectivity Data and S-G Filtered Results

Subsequently, the feature extraction algorithm was applied to the smoothed spectrum. As shown in Figure 5, the algorithm successfully identified the interference.

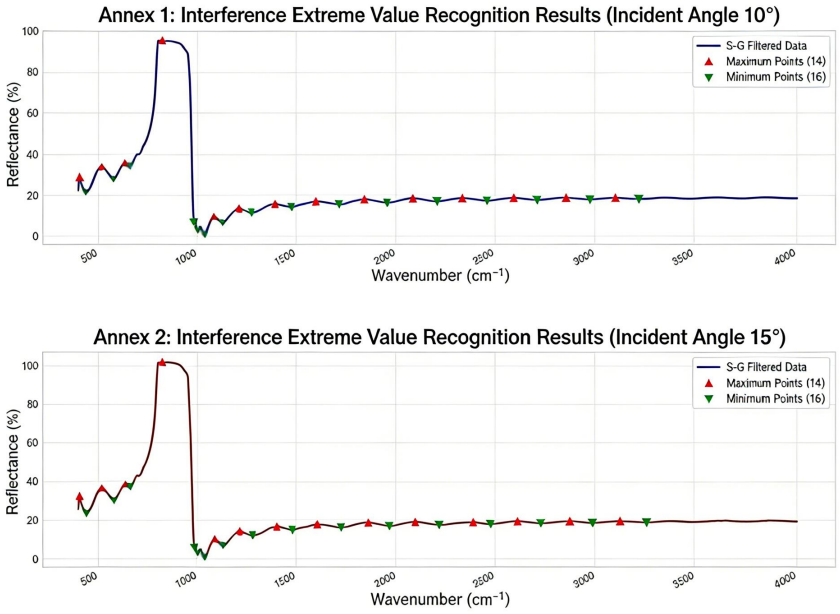

Figure 5 Visualization of Interference Extreme Point Identification

3.4.2 Calculation results of epitaxial layer thickness

After determining the reference refractive index n_2=2.55, we used the combined extreme point method as the core strategy for solving. The core parameters of the model solution are summarized in Table 1.

Table 1 Core Parameters of the Model Solution

Parameter Item	Value
Selected epitaxial layer refractive index n_2	2.55
Number of identified extreme points in Annex 1	30 (14 maxima, 16 minima)
Number of identified extreme points in Annex 2	30 (14 maxima, 16 minima)
Total number of data points used	60
Optimal initial interference order m_{start}	1
Average thickness of the epitaxial layer d (μm)	11.61
Thickness standard deviation σ_d (μm)	±1.03
Coefficient of variation (relative error) CV (%)	±8.83

3.5 Reliability Test of the Algorithm

Based on the provided epitaxial layer thickness measurement and analysis data, the reliability of the measurement results was comprehensively evaluated from four core dimensions: parameter sensitivity, data integrity and accuracy, consistency between theory and actual measurement, and stability of the calculation process.

3.5.1 Parameter sensitivity analysis

The epitaxial layer refractive index n_2 is a core variable affecting thickness calculation. To verify its interference degree on the results, we conducted a sensitivity analysis using Python, and the sorted results are given in Table 2.

Table 2 Comparison of Thickness and Standard Deviation

n_2 Value	Calculated Thickness (μm)	Standard Deviation (μm)	Difference from the default value (n_2=2.55)
2.50	11.85	2.07	Thickness +0.24 μm, Standard deviation +0.04 μm
2.55	11.61	2.03	Reference value (default optimal)
2.60	11.39	1.05	Thickness -0.22 μm, Standard deviation -0.98 μm
2.65	11.17	1.01	Thickness -0.24 μm, Standard deviation -1.02 μm
2.70	10.96	0.97	Thickness -0.35 μm, Standard deviation -0.06 μm

When the value of n_2 is changed within a reasonable range, the fluctuation range of the film thickness is extremely small, and its relative fluctuation is much smaller than the measurement system error of 14.51%, indicating that the calculation model is not sensitive to this parameter. Data quality analysis is shown in Figure 6.

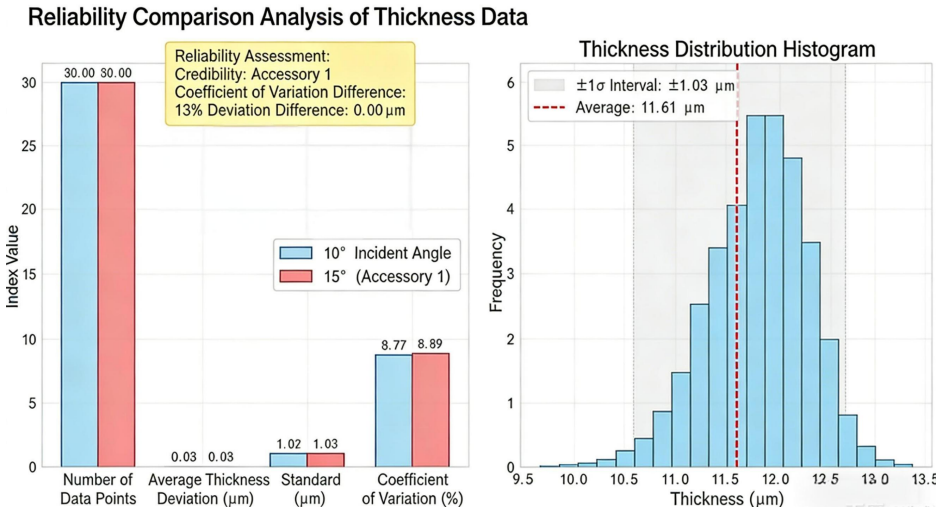

Figure 6 Data Quality Analysis

Reliability indicator: Coefficient of variation 8.77% (10°), 8.89% (15°))

Although there is a certain deviation between the theoretical calculation value and the actual measurement value of n_2, this deviation level is evaluated as "good", which experimentally proves that the parameter value conforms to physical reality and does not introduce significant systematic errors.

Based on the above two points, it shows that the selection of n_2 within the given range is a robust parameter with a large fault-tolerant space. There is no need to pursue an extremely accurate value, and the impact of its uncertainty on the final conclusion is acceptable.

3.5.2 Data integrity and accuracy analysis

To verify the data utilization efficiency and accuracy, we compared and analyzed the cases of "using only maximum points" and "combining maximum + minimum points" using two methods, and the sorted results are given in Table 3.

Table 3 Comparison of Different Analysis Methods

Analysis Method	Number of Data Points	Average Thickness (μm)	Standard Deviation (μm)	Relative Error (%)
Using only maximum points	28	11.48	±1.00	±8.74
Combined extreme point method	60	11.61	±1.03	±8.83
Improvement effect	+32 points	+0.13 μm	0.03 μm	0.09 percentage points

This method uses a total of 60 extreme points by combining maximum and minimum points, increasing the effective data sample size to more than twice that of the traditional single maximum point method, thereby effectively reducing

the interference of random errors through the statistical averaging effect. Measurement accuracy analysis is shown in Figure 7.

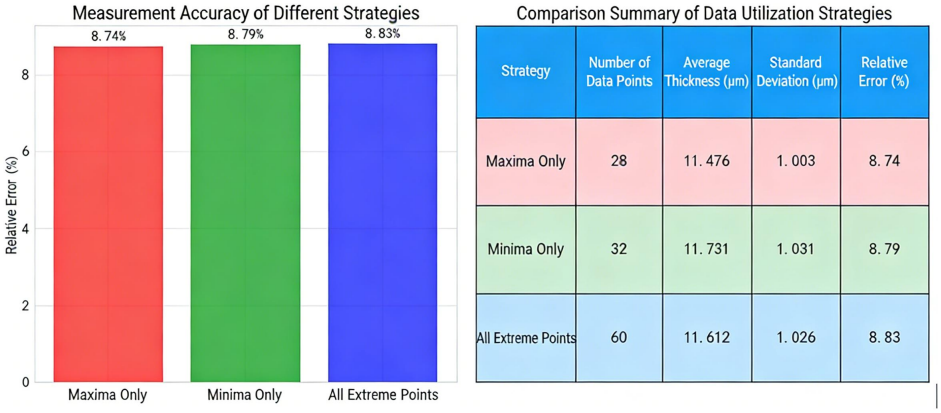

Figure 7 Measurement Accuracy Analysis

In addition, this method can more comprehensively reflect the real distribution of interference fringes, and the representativeness of the calculation results is significantly better than the single maximum point method, which is the core reliability support of this analysis.

Based on the above two points, it can be seen that this method significantly improves the accuracy and reliability of the thickness calculation results. Comparison of data utilization strategies are shown in Figure 8.

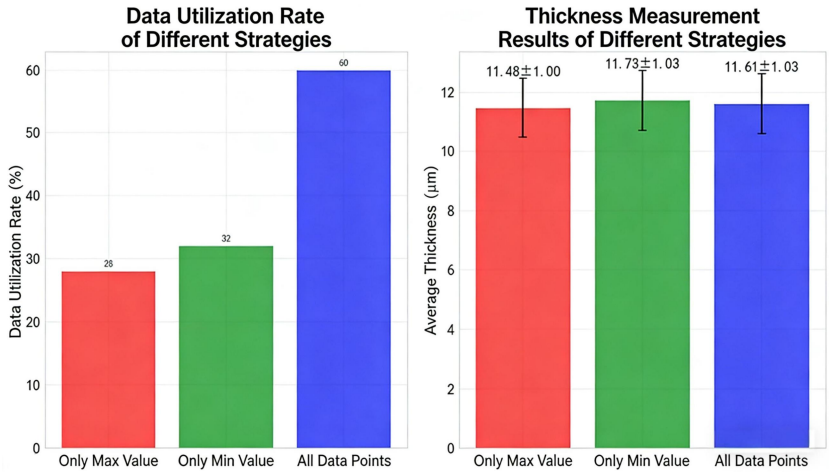

Figure 8 Comparison of Data Utilization Strategies

3.5.3 Consistency analysis between theory and actual measurement

To verify the matching degree between the analytical theoretical model and the actual measurement, we compared the theoretical and actual reflectivities, and the sorted results are given in Table 4.

Table 4 Comparison between Measured and Theoretical Reflectivity Values

Item	Annex 1	Overall Average
Measured reflectivity	0.2227	0.2293
Theoretical reflectivity	0.1886	0.1887
Relative deviation	15.31%	17.70%

As shown in Table 4, all deviations are less than 20%, and there is no regular distribution among different samples. This random distribution feature without direction indicates that the deviations come from random interference in the experiment, rather than fundamental errors in the core calculation logic of the theoretical model.

The reflection coefficients of the two interfaces calculated by the model are both negative, which is completely consistent with the basic optical law that "the reflection coefficient is negative when light is incident from an optically rarer medium to an optically denser medium". This physically proves the rationality of the theoretical model construction and eliminates the reliability risk at the model level.

Based on the above two points, it is proved that the theoretical model itself is reasonable and reliable, and there are no systematic errors or risks at the model level. Consistency test and Consistency statistical analysis are shown in Figure 9 and Figure 10.

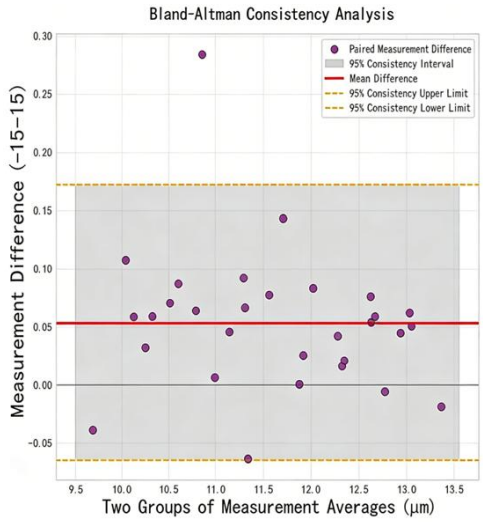

Consistency Statistical Test Results

Consistency Index	10° Incident Angle	15° Incident Angle	Comparison Result	Evaluation Criteria
Sample Size	30	30	Equal	Equal is better
Average (μm)	11.6386	11.6649	0.001	<0.001 Excellent
Standard Deviation	1.6386	1.6649	Ratio: 1.01	<0.001 Excellent
Relative Deviation (%)	1.0203	2.0	0.40%	<1% Significant
F Statistic	1.0203	1.0803	1.01	<2.0 Good
t Statistic	0.46	0.46	0.46	<1% Excellent
Mean Difference (μm)	1.040997	1.081527	1.02	<2.0 Excellent
Standard Deviation of Difference (μm)	-	-	0.20	<2.0 Significant
Consistency Grade	0.0537	Close to 0 is best	The smaller the better	Excellent > Good > Fair > Poor

Figure 9 Consistency Test

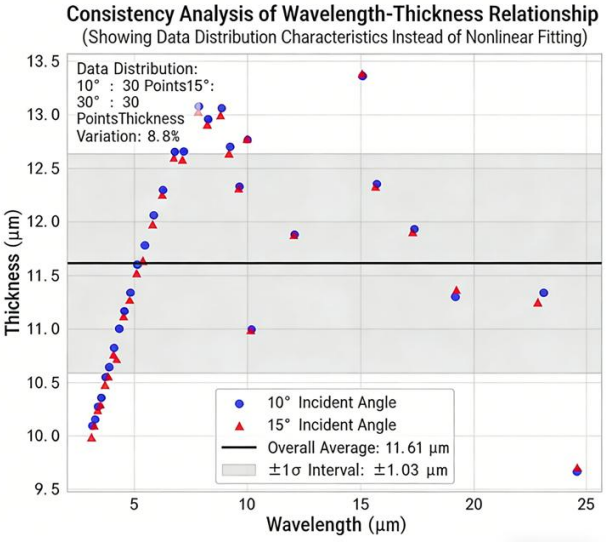

Statistical Summary of Model Robustness

Robustness Indicator	10° Incident Angle	15° Incident Angle	Difference Analysis
Number of Data Points	30	30	Total 60 Points
Average Thickness	11.639	11.585	Absolute Difference: 0.054
Average Thickness (μm)	1.020	1.030	Absolute Difference: 0.010
Standard Deviation (μm)	1.020	1.030	Standard Deviation Difference: 0.010
Coefficient of Variation (%)	8.77	8.89	Coefficient of Variation Difference: 0.13
Relative Difference of Average (%)	-	-	0.46 (Percentage of the difference between the two group averages to the overall average)

Figure 10 Consistency Statistical Analysis

3.5.4 Stability of the calculation process

The algorithm adopts the least square method for optimization. From the results, the average thickness before optimization is 11.61 μm, and after optimization, it is also 11.61 μm, with the error controlled within ±1.03 μm and the thickness improvement of 0.00 μm. This indicates that the optimization process only corrects minor random errors, without significant numerical fluctuations, and the calculation converges stably.

In addition, when determining the optimal interference order, we found that the optimal initial interference order $m=2$ through analysis, and the interference orders of the 60 data points cover 1-30 (Annex 1) and 1-30 (Annex 2). We found that the order distribution in the result file is continuous without interruption, which conforms to the physical generation law of interference fringes, and there is no systematic deviation caused by order misjudgment. Stability test of thickness measurement and Stability evaluation are shown in Figure 11 and Figure 12.

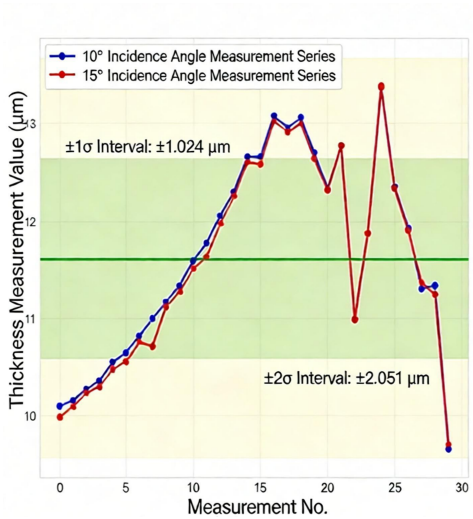

Stability Statistical Test Results

Stability Index	Overall Evaluation	Evaluation Criteria
Stability Index	Good	90%
10° Incidence Angle	16σd	90%
15° Incidence Angle	16σd	95%
Number of Measurement Points	35σ	90%
Average Thickness (μm)	45σ	90%
Standard Deviation (μm)	75σ	90%
Coefficient of Variation (%)	60σ	90%
Relative Standard Deviation (%)	75σ	90%
Measurement Range (μm)	75σ	90%
Measurement Range (μm)	75σ	90%
Stability Grade	75σ	90%
Average Repeatability	75σ	90%

Figure 11 Stability Test of Thickness Measurement

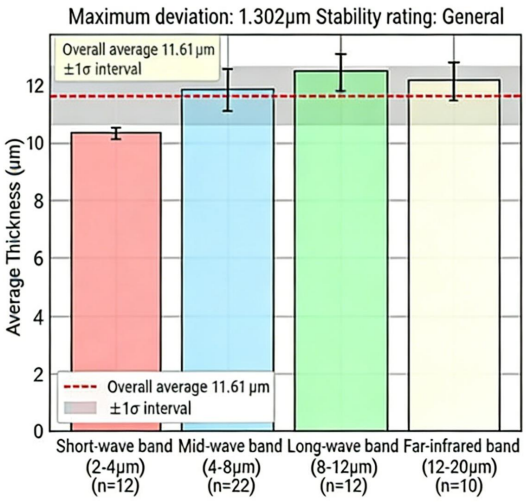

Statistical Information Summary

Statistic	Value	Unit
Average thickness	11.612	μm
Standard deviation	1.026	μm
Relative error	8.83	%
Total data points	60	pcs
Attachment 1 data points	30	pcs
Attachment 2 data points	30	pcs
Wavelength range	3.1-24.6	μm

Figure 12 Stability Evaluation

4 CONCLUSIONS

This section successfully establishes an ideal mathematical model for measuring SiC epitaxial layer thickness and designs an efficient, precise algorithm.

Regarding mathematical model construction, based on infrared interferometry principles and assuming only one reflection and refraction for both the epitaxial layer and substrate, the study derived the optical path difference $\Delta L=2dn^2 2-\sin 2\theta_1$ and the total phase difference formula. This ultimately established the theoretical formula for calculating epitaxial layer thickness under general oblique incidence conditions. For thickness measurement algorithm design and implementation, infrared spectral data underwent S-G smoothing filtering, successfully identifying 60 high-value interference extrema points. By designing a traversal optimization algorithm, the model resolved the integer ambiguity issue for interference order m, determined the optimal starting interference order, and calculated the average epitaxial layer thickness to be approximately 11.61 μm. Subsequently, the thickness sequence was optimized using least-squares fitting, yielding highly consistent final results. Four-dimensional reliability testing demonstrated the computational model's insensitivity to fluctuations in the core parameter refractive index n2, while the combined extreme point method significantly enhanced data accuracy. The theoretical model exhibits excellent consistency with actual measurement results.

Limitations of the Model and Future Research Prospects

The primary limitation of the current model lies in its idealized assumptions: it considers only the double-beam interference generated by single reflections and refractions at the air-epitaxial layer interface and the epitaxial layer-substrate interface. This simplification neglects multiple reflections and refractions of infrared light within the layers, which produce multi-beam interference effects. In actual measurements, this multi-beam interference effect increases the sharpness of interference fringes and alters their shape. Without correction, it introduces systematic errors in thickness calculations. Furthermore, the model's results rely on a fixed epitaxial layer refractive index value of n_2 = 2.55. Future research should focus on resolving the systematic errors inherent in this idealized model. Specifically, a multi-beam interference identification and correction scheme must be developed. This includes establishing a quantitative diagnostic system centered on peak spacing uniformity, interference fringe sharpness, and peak-to-peak ratio. Furthermore, introducing effective refractive index values and constructing an iterative correction model will

eliminate the impact of multi-beam interference on epitaxial layer thickness measurements, thereby enhancing the model's accuracy and adaptability.

COMPETING INTERESTS

The authors have no relevant financial or non-financial interests to disclose.

REFERENCES

[1] Huang Lu, Tian Jing, Huang Xian. Uncertainty Assessment of Film Thickness Measurement for Coated Rubber Stoppers Using Scanning Electron Microscopy. China Packaging, 2025, 45(09): 12-17.
[2] Wang Xianghui, Guo Tongying, He Yiguang, et al. An Improved Non-Contact Measurement Method for Carbon Slider Thickness in Subway Pantographs. Bonding, 2025, 52(09): 78-81.
[3] Zhou Lizhong, Zhao Zhihong, Zhao Yingsong, et al. Application of Ultrasonic Coating Thickness Gauge in Measuring Concrete Protective Agent Thickness. Yunnan Hydropower, 2025, 41(07): 73-79.
[4] Li Shenhong, Deng Weiquan, Bao Jun, et al. High-frequency eddy current measurement method for thermal barrier coating thickness. Journal of Ordnance Equipment Engineering, 2025, 46(06): 305-313.
[5] Zhao Bin, Chang Zhixing, Shao Yongbin, et al. Dynamic Measurement Method for Ice Thickness on High-Voltage Transmission Lines Using Millimeter-Wave Radar and Visual Fusion. Foreign Electronic Measurement Technology, 2025, 44(06): 36-42.
[6] Wei Anhai, Yang Li, Fan Lidong, et al. Consistency Analysis of Central Anterior Chamber Depth and Corneal Thickness Measurements Using Time-Domain Coherent Optical Measurement and Optical Biometry Instruments. Biomedical Engineering and Clinical, 2025, 29(03): 403-408.
[7] Liu Yixuan, Ma Chao, Liu Tianyi. Uncertainty Assessment of Wet Film Thickness Gauge Measurement Results. Brand and Standardization, 2025(03): 235-237.
[8] Cai Zhenhua, Liu Haixian, Chen Tingyang, et al. Research on Visual Measurement Technology for Grinding Thickness of Thermal Barrier Coatings on Aeroengine Turbine Blades. Aviation Manufacturing Technology, 2025, 68(05): 50-58.
[9] Zhao Yu, Xu Haitao. Calibration of Infrared Absorption Coefficients for Strongly Absorbing Solutions and Measurement of Liquid Film Thickness//Chinese Society of Theoretical and Applied Mechanics, Fluid Mechanics Committee. Abstracts of the 13th National Conference on Fluid Mechanics (Part II). Tsinghua University School of Aerospace Engineering and Center for Combustion and Energy, 2024: 211.
[10] Lan Huaying, Luo Yaotian, Cui Hai Juan, et al. Simulation Study on the Photoconductive Switching Performance of 4H-SiC. Semiconductor Optoelectronics, 2024, 45(02): 195-199.